

# Co-Doping TiO<sub>2</sub> Nanoparticles with Phosphorus and Nitrogen- A way to Enhance the Visible Light Driven Charge Separation

Md. Hussain Basha, N.O. Gopal\*

**Abstract:** Codoping TiO<sub>2</sub> with nonmetals is one of the strategies that is used to make these materials sensitive to visible light. In this work, we obtained phosphorus and nitrogen codoped TiO<sub>2</sub> nanoparticles by sol-gel method using H<sub>3</sub>PO<sub>4</sub>, NH<sub>4</sub>OH and Ti (IV) isopropoxide as precursors. As prepared sample were calcined at different temperatures, and the obtained samples were characterized by using different techniques. XRD analysis reveals the retarded phase transition by increased thermal stability and decreased particle size due to codoping. UV-Vis absorption spectra of the co-doped samples show redshift in their absorption edge due to doping of nitrogen and phosphorus. From XPS measurements, it is clear that nitrogen enters into interstitial sites of titania and phosphorus exists in a pentavalent oxidation state by replacing part of lattice Ti<sup>4+</sup> by the formation of Ti-O-P bonds. Low temperature (77K) EPR studies with in situ visible high irradiation (>400nm) on the samples heated at different temperatures exhibit signals due to N<sup>•</sup>, NO and the radicals formed due to photogenerated holes trapped at different sites in these samples. Effect of heating temperature on these EPR signals has been studied in detail. EPR data reveals the enhanced charge separation as evidenced by the increased hole signal intensity and this enhanced charge separation plays important role in the photocatalytic activity of these samples.

**Keywords:** Codoping TiO<sub>2</sub>, XRD, UV-Vis, N<sup>•</sup>, NO, (77K) EPR, Ti-O-P bonds, H<sub>3</sub>PO<sub>4</sub>, NH<sub>4</sub>OH and Ti (IV), redshift

## I. INTRODUCTION

Visible light active photocatalytic materials effectively utilize sunlight and promises widespread applications related to degradation of toxic chemicals with low energy consumption. In this aspect, there has been growing interest in the development of visible light active photocatalytic materials for environmental remediation purpose. Titanium dioxide (TiO<sub>2</sub>) continues to be one of the most promising and investigated materials in the fields of photocatalysis and solar energy conversion [1-5]. The metal oxide offers chemical versatility displaying both semiconducting and catalytic activity coupled to excellent chemical stability. An intrinsic property of TiO<sub>2</sub>, as well as its greatest disadvantage is that, as a wide band gap semiconductor (3.2 eV for anatase) it requires energy greater than 3.1-3.2 eV to excite electrons from the valence band to the conduction band. Therefore, its implementation in visible light sensitive solar energy applications, and photocatalytic applications as commonly envisioned is limited. In this aspect, most successful strategy to narrow the band gap of TiO<sub>2</sub>, so that it absorbs visible light is to introduce doping elements in to its crystal lattice.

Revised Version Manuscript Received on July 26, 2016.

\* corresponding author

Md. Hussain Basha, Department of Physics, Vikrama Simhapuri University P.G. Centre, Kavali (Andhra Pradesh). India.

N.O. Gopal\*, Department of Physics, Vikrama Simhapuri University P.G. Centre, Kavali (Andhra Pradesh). India.

Doping is a promising approach to reduce the absorption threshold of titanium dioxide (TiO<sub>2</sub>) and bring it from the UV to the visible region [6]. An intense research activity has been recently devoted to the preparation and characterization of titanium dioxide (TiO<sub>2</sub>) materials singly doped and codoped with nonmetal impurities [7-13]. The goal is to produce an active photocatalyst, which can work under visible light, rather than UV irradiation, so that sunlight can be more efficiently used in photocatalysis. One of the most promising and widely investigated systems in this respect is phosphorus doped titanium dioxide, which shows a significant catalytic activity in various reactions performed under visible light irradiation. It is reported that the phosphate – modification of titania can result in the improvement of its thermal stability and photocatalytic activity, offering an excellent photocatalytic activity in visible light [14-16]. Further, since the pioneering discovery by Asahi et al [17], masses of works of N-doped TiO<sub>2</sub> have appeared. Various synthesis methods have been reported, such as direct amination of TiO<sub>2</sub>, solvo thermal approach and sol-gel process [18,19] and the origin of the visible light photocatalytic activity of N-doped TiO<sub>2</sub> and the influence of N dopant concentration on the photocatalytic activity are studied [20,21]. Very recently, codoping TiO<sub>2</sub> with non-metals is found to be an effective method to improve the visible light activity of TiO<sub>2</sub>-based photocatalysts. In this report, we present our investigations on phosphorus and nitrogen codoped TiO<sub>2</sub> nanoparticles prepared by sol-gel method and the effect of calcination temperature on the physiochemical properties of dopants, which plays an important role in photocatalytic properties of TiO<sub>2</sub>.

## II. EXPERIMENTAL METHODS

### 2.1. Preparation of the catalyst

Titanium (IV) isopropoxide, phosphoric acid and ammonium hydroxide were used as precursors for TiO<sub>2</sub>, phosphorus and nitrogen respectively. All the chemicals were of reagent grade and used as received. Phosphorus and nitrogen co-doped TiO<sub>2</sub> (P,N-TiO<sub>2</sub>) nanoparticles were prepared by sol-gel method. For P,N-TiO<sub>2</sub>, a mixture of ethyl alcohol, DDwater, NH<sub>4</sub>OH and H<sub>3</sub>PO<sub>4</sub> was cooled to ice cold temperature (<4 °C) and Ti(IV)isopropoxide was added drop by drop to the above mixture at ice cold temperature under vigorous stirring. After adding Ti(IV) isopropoxide, the mixture was kept for continuous stirring at room temperature for the complete hydrolysis of Ti(IV) isopropoxide. The gels obtained in this way were aged for 24 h and then centrifuged to separate the precipitates. The powders were then dried at room temperature. The as prepared xerogel samples were calcined at 400, 500, 600,

and 700 °C for 4 h at the rate of 3 °C/min.

### 2.2. Materials Characterization

The crystallinity and particle size of all the prepared samples were investigated by the X-ray diffraction patterns collected in the range 20-80° (2θ) using a Rigaku X-ray diffractometer (XRD) operating with Cu Kα radiation at 40 kV and 100 mA. The UV-Vis reflectance absorption spectra were obtained at room temperature in air within the range 250-800 nm for the dry-pressed disk samples using BaSO<sub>4</sub> as the reference sample on a Shimadzu UV-2550 UV-vis spectrophotometer equipped with an integrating sphere assembly. X-ray photoelectron spectroscopy (XPS) characterizations were performed using a Kα system (Thermo scientific) with monochromatic Al Kα excitation and a charge neutralizer. Scanning electron microscopy (SEM) images were obtained from a JEOL JSM7000F field emission scanning electron microscope. EPR spectra were obtained at X-band using a Bruker EMX spectrometer equipped with a Bruker TE<sub>102</sub> cavity. The microwave frequency was measured with a Hewlett-Packard 5246 L electronic counter. The instrument settings are shown in the figure legend.

## III. RESULTS AND DISCUSSION

### 3.1. Crystal structure analysis

XRD analysis was performed to investigate the structural phases and crystallite sizes of the samples. The crystal structure of TiO<sub>2</sub> depends on the temperature of heat treatment. Figure 1 shows the XRD patterns of P,N-TiO<sub>2</sub> sample heated at different temperatures. All the observed peaks can be fully indexed of anatase crystalline phase of TiO<sub>2</sub>. The average particle size of all the samples at different temperatures was estimated by profile fitting (using XRD analysis software jade R5) the (101) peak of anatase. With increasing temperature, the increase in the intensity and sharpness of the diffraction peaks indicates the increased crystallinity and particle

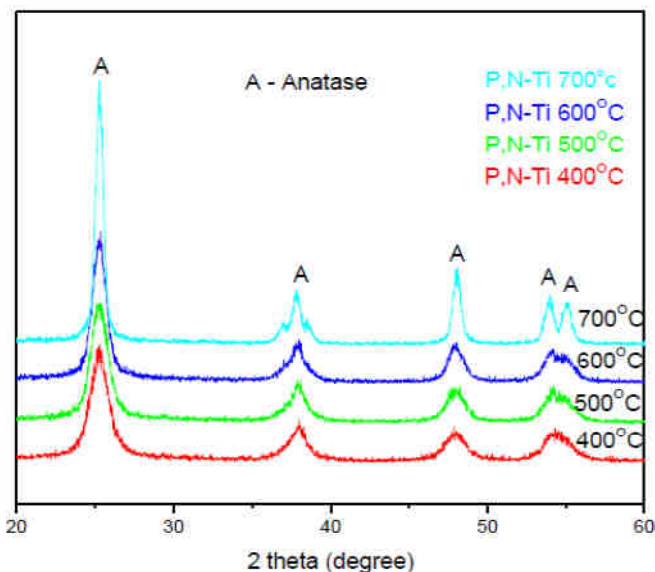


Figure 1. XRD patterns of P, N-TiO<sub>2</sub> samples heated at different temperatures.

Size of the samples. The particle size of P,N- TiO<sub>2</sub> sample at 400 °C is 5.7nm, which increases to 20.1nm at 700 °C.

Compared to undoped sample (data not shown), which shows rutilization at 600 °C, XRD analysis of P,N- TiO<sub>2</sub> reveals the retarded phase transition by increased thermal stability and decreased particle size due to codoping. Figure 2 shows the SEM image of P,N- TiO<sub>2</sub> sample heated at 700 °C, which depicts the uniform distribution of nanoparticles with an average particle size of 22 nm, which is in agreement with the particle size obtained from XRD data.

### 3.2. UV-Vis diffuse reflectance spectra

The optical properties of all the prepared samples have been investigated by measuring the UV-Vis reflectance absorption spectra of the samples. Figure 3 shows the reflectance absorption

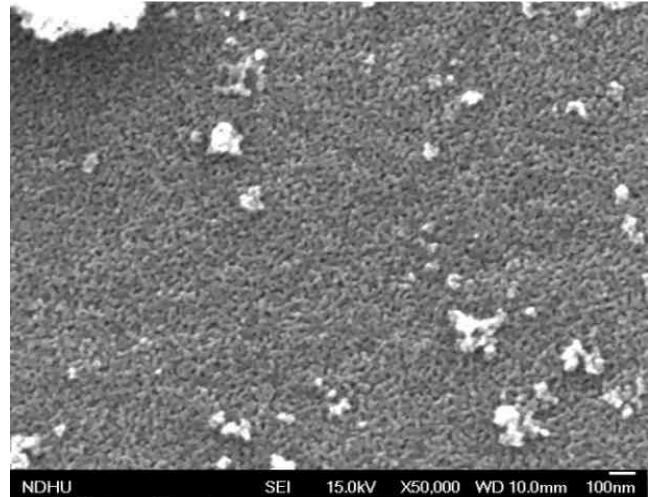


Figure 2. SEM micrograph of P,N-TiO<sub>2</sub> sample heated at 700 °C.

spectra of P,N-TiO<sub>2</sub> samples heated at different temperatures. As shown in figure, the absence of absorption shoulder around 450 nm, which is characteristic of substitutional nitrogen in the oxygen site indicates that the doped nitrogen in these samples may be in the interstitial sites. The absorption edge of P,N-TiO<sub>2</sub> sample exhibits red shift (Figure 3 inset) with increase in temperature, which is due to doping of phosphorus and nitrogen into titanium sites. The observed red shift in the present work is in good agreement with earlier reports [14-16].

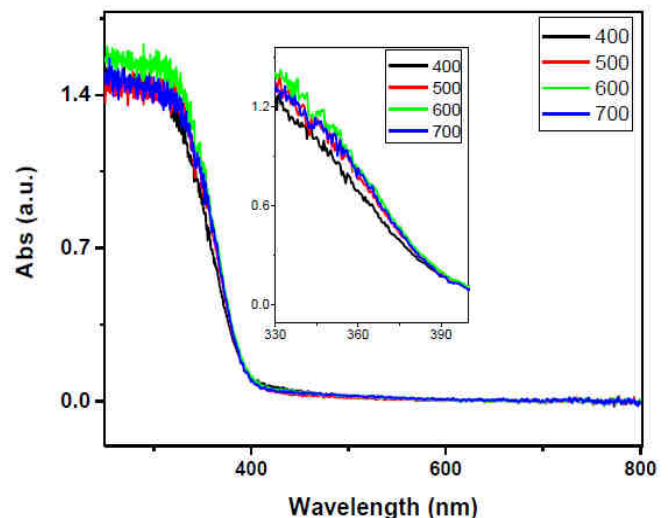


Figure 3. UV-visible diffuse reflectance spectra of P,N-TiO<sub>2</sub> samples heated at different temperatures.

### 3.3. XPS Studies.

XPS measurements have been carried out to understand the chemical state of the doped species in P,N-TiO<sub>2</sub> samples. The XPS spectrum shows the peaks due to N, P, Ti and O, which indicates the incorporation of P and N into the TiO<sub>2</sub> crystal lattice. Figure 4. shows the N 1s XPS spectrum of P,N-TiO<sub>2</sub> sample heated at 400 °C exhibiting a peak at around 401.07 eV, which is due to interstitial nitrogen doping. XPS peak of N 1s has been under debate for a long time. The N 1s peak observed in our sample is in the range of previously reported nitrogen doped titanias [22-25], which is higher than that of Ti-N appeared around 397.5 eV [26], and lower than that of hyponitrite type nitrogen around 404 eV [27]. The observed N1s peak around 401.07 eV may be ascribed to the interstitial nitrogen [28-31].

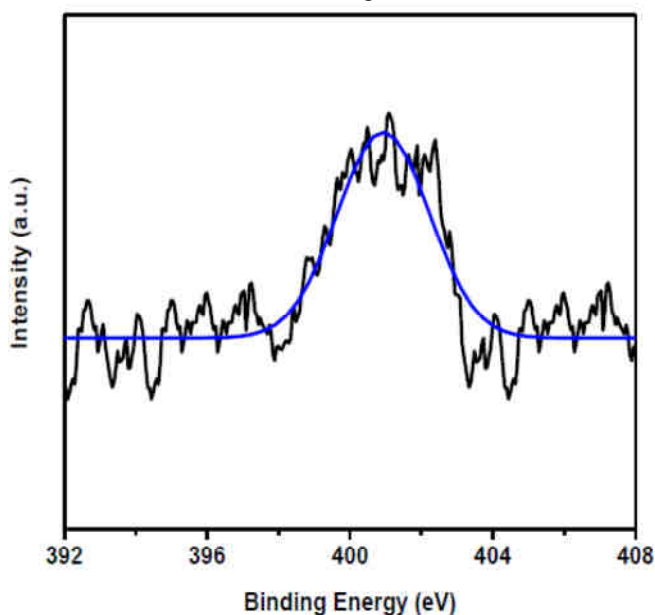


Figure 4. N 1s X-ray photoelectron spectrum and its peak fitting of P,N-TiO<sub>2</sub> sample heated at 400 °C

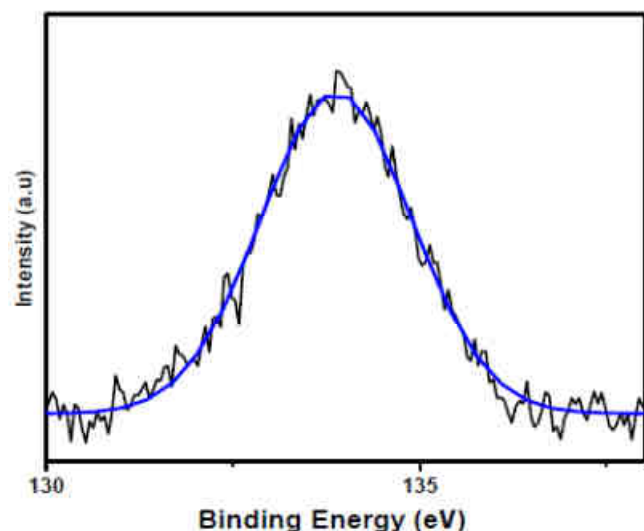


Figure 5. P 2p X-ray photoelectron spectrum of P,N-TiO<sub>2</sub> sample heated at 600 °C.

As shown in Figure 5, the P 2P<sub>3/2</sub> peak is observed at 133.7 eV. Based on earlier reports by Zheng et.al. [32,33], Lv et. al. [34] and our earlier report [14] on phosphorus doped TiO<sub>2</sub>, and also on the ionic radii concern (0.67 for Ti<sup>4+</sup> and

0.38 for P<sup>5+</sup>), we suggest that phosphorus substitutes into Ti<sup>4+</sup> sites in pentavalent oxidation state (P<sup>5+</sup>) by the formation of Ti-O-P bonds.

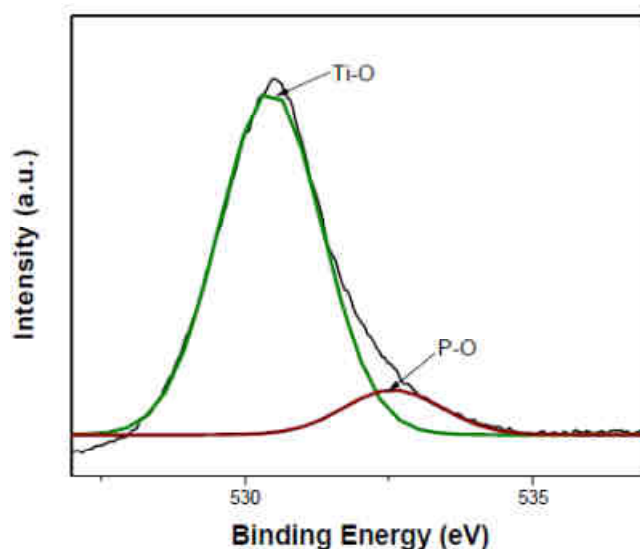


Figure 6. Peak fitting for the XPS spectrum of P,N-TiO<sub>2</sub> sample heated at 600 °C in the binding energy range of O 1s.

The formation of Ti-O-P bonds in the crystal lattice may be the reason for the observed red shift in the UV-vis spectrum. The O 1s peak for the P,N-TiO<sub>2</sub> sample heated at 600 °C and its peak fitting are shown in Figure 6. The observed peak is fitted by two peaks pertaining to Ti-O and P-O bonds, which further supports the substitution doping of phosphorus into Ti<sup>4+</sup> sites.

### 3.4. Electron Paramagnetic Resonance:

EPR is an exceptional tool to study the radicals formed due to trapped photogenerated charge carriers even at very low concentrations. Using low temperature EPR, the dynamics and the kinetics of the photogenerated electron and hole species and their interactions can be studied [35,36]. At room temperature, EPR spectrum of P,N-TiO<sub>2</sub> samples do not exhibit any signals indicating that the nitrogen in these samples is in diamagnetic state (N<sup>-</sup>). Figure 7a shows the 77K EPR spectra of P,N-TiO<sub>2</sub> sample heated at different temperatures. The sample heated at 400 °C exhibit signals due to NO radicals (g = 1.999; A = 31.5 G) [37,38] and the intensity of this NO signal goes on decreasing with increasing calcinations temperature. EPR spectra of P,N-TiO<sub>2</sub> samples at 77K with visible light (>400 nm) irradiation are shown in Figure 7b. In addition to NO signal, the EPR spectrum of the samples heated upto 400 °C with irradiation exhibit the signals due to N<sup>•</sup> (g = 2.005; A = 32 G) formed [37,38] by the conversion of diamagnetic N<sup>-</sup> into paramagnetic N<sup>•</sup> [37-39] and the signal due to trapped photogenerated holes represented by signal A, which is due to [Ti<sup>4+</sup> O<sup>2-</sup> Ti<sup>4+</sup> O<sup>-•</sup>] radical with a set of g values around g<sub>1</sub> = 2.0265, g<sub>2</sub> = 2.0113 and g<sub>3</sub> = 2.0039 formed due to photogenerated holes trapped at the lattice oxygen atoms located in the surface/subsurface layer [14,36,40]. The intensity of NO and N<sup>•</sup> signals decreases with increasing temperature, where as the intensity of [Ti<sup>4+</sup> O<sup>2-</sup> Ti<sup>4+</sup> O<sup>-•</sup>] signal increases up to 600 °C. In the sample heated at

700 °C, the NO and N<sup>•</sup> signals are almost

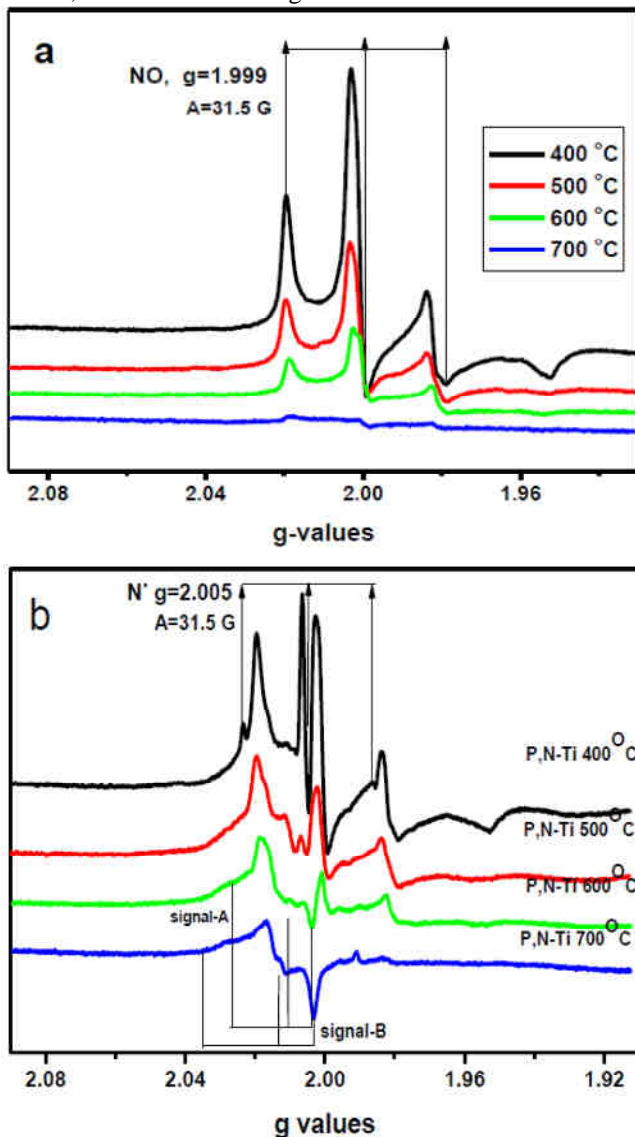


**Figure 7. EPR spectra at 77K for P,N-TiO<sub>2</sub> sample heated at different temperatures (a) without irradiation and (b) visible light ( $\lambda > 400$  nm) irradiation. Instrument settings: microwave frequency, 9.5400 GHz; microwave power, 3.16 mW; modulation amplitude, 2 G at 100 kHz.**

disappeared with the appearance of new signal represented by signal B, which is due to [Ti<sup>4+</sup> O<sup>2-</sup> Ti<sup>4+</sup> O<sup>•</sup>] radical with a set of g values around  $g_1 = 2.0347$ ,  $g_2 = 2.0141$  and  $g_3 = 2.0031$  formed due to holes trapped at different oxygen sites compared to signal A. All the observed signals are in agreement with previous studies [14,35,36,40] and these photogenerated radicals would be useful for visible light activated photocatalytic applications.

#### IV. CONCLUSIONS

By using sol-gel method, phosphorus and nitrogen codoped TiO<sub>2</sub> nanoparticles were prepared and investigated by various techniques. From the observed results, it is clear that phosphorus and nitrogen are doped into the Titania lattice. XRD analysis reveals the decreased particle size and increased thermal stability due to codoping. UV-Vis absorption spectra of the co-doped samples show redshift in their absorption edge due to doping of nitrogen and

phosphorus. From XPS measurements, it is clear that nitrogen enters into interstitial sites, and phosphorus exists in a pentavalent oxidation state by replacing part of lattice Ti<sup>4+</sup> by the formation of Ti-O-P bonds. Low temperature (77K) EPR studies with in situ visible-irradiation (>400nm) on the samples heated at different temperatures exhibit signals due to N<sup>•</sup>, NO and the radicals formed due to photogenerated holes. EPR data reveals the enhanced charge separation as evidenced by the increased hole signal intensity and this enhanced charge separation may plays an important role in the photocatalytic activity of these samples.

#### ACKNOWLEDGEMENT

The authors would like to thank the Council of Scientific and Industrial Research (CSIR), New Delhi, India for financially supporting this research under scheme No. 03(1364)/16/EMR-II.

#### REFERENCES

1. J. Schneider, M. Matsuoka, M. Takeuchi, J. Zhang, H. Yu, M. Anpo, D. W. Bahnemann, Chem. Rev. 114 (19) (2014) 9986.
2. D. Flak, E. Coy, G. Nowaczyk, L. Yate, S. Jurga, RSC Adv. 5 (2015) 85152.
3. G. Wang, X. Xiao, W. Li, Z. Lin, Z. Zhao, C. Chen, C. Wang, Y. Li, X. Huang, L. Miao, C. Jiang, Y. Huang, X. Duan, Nano Lett. 15 (2015) 4698.
4. M. Miyauchi, H. Irie, M. Liu, X. Qiu, H. Yu, K. Sunada, K. Hashimoto, J. Phys. Chem. Lett. 7 (1) (2016) 84.
5. H. Park, H. Kim, G. Moon, W. Choi, Energy Environ. Sci. 9 (2016) 433.
6. R. Asahi, T. Morikawa, H. Irie, T. Ohwaki, Chem. Rev. 114 (19) (2014) 9852.
7. Z. He, W. Que, J. Chen, X. Yin, Y. He, J. Ren, ACS Appl. Mater. Interfaces. 4 (12) (2012) 6826.
8. P. Kavitha, S. Morrow, C. Han, M. Pelaez, X. He, D. D. Dionysiou, H.M. Hwang, Environ. Sci. Technol. 47 (17) (2013) 9996.
9. C. Sun, D. J. Searles, J. Phys. Chem. C. 117 (50) (2013) 26459.
10. M. V. Dozzi, L. Artiglia, G. Granozzi, B. Ohtani, E. Selli, J. Phys. Chem. C. 118 (44) (2014) 25589.
11. J. Zhao, L. Zhang, W. Xing, K. Lu, J. Phys. Chem. C. 119 (14) (2015) 7737.
12. Y. Shao, C. Cao, S. Chen, M. He, J. Fang, J. Chen, X. Li, D. Li, Appl. Catal. B: Environ. 179 (2015) 351.
13. A.E. Giannakas, M. Antonopoulou, C. Daikopoulos, Y. Deligiannakis, I. Konstantinou, Appl. Catal. B: Environ. 184 (2016) 54.
14. N. O. Gopal, H.H. Lo, T.F. Ke, C.H. Lee, C.C. Chou, J.D. Wu, S.C. Sheu, S.C. Ke, J. Phys. Chem. C, 116 (2012) 16197.
15. J. Niu, P. Lu, M. Kang, K. Deng, B. Yao, X. Yu, Q. Zhang, Appl. Surf. Sci. 319 (2014) 106.
16. X. Yue, J. Yinshan, Li. Fangfei, X. Maosheng X. Bing, L. Yanjuan, Applied Surface Science.289 (2014) 315.
17. R. Asahi, T. Morikawa, T. Ohwaki, K. Aoki, Y. Taga, Science 2001, 293, 269.
18. C. Burda, Y. Lou, X. Chen, A.C.S. Samia, J. Stout, J. L. Gole, Nano Lett. 3 (2003)- 1049-1051.
19. N.S. Chaudhari, S.S. Warule, S. A. Dhanmane, M.V. Kulkarni, M. Valant, B. B.Kale, Nanoscale 5 (2013) 9383-9390.
20. Z. Zhang, Z. Luo, Z. Yang, S. Zhang, Y. Zhang, Y. Zhou, X. Wang, X. Fu, RSC Advances 3 (2013) 7215-7218.
21. K. Yang, Y. Dai, B. Huang, J. Phys. Chem. C 111 (2007) 12086-12090.
22. Y. Cong, J. Zhang, F. Chen, M. Anpo, J. Phys. Chem. C 111 (2007) 6976.
23. R. Nakamura, T. Tanaka, Y. Nakato, J. Phys. Chem. B 108 (2004) 10617.
24. J.L. Gole, J.D. Stout, C. Burda, Y. Lou, X. Chen, J. Phys. Chem. B 108 (2004) 1230.
25. X. Chen, C. Burda, J. Phys. Chem. B 108 (2004) 15446.
26. N.C. Saha, H.G. Tompkins, J. Appl. Phys. 72 (1992) 3072.
27. Y. C. Hong, C. U. Bang, D.H. Shin, H.S. Uhm, Chem.Phys.Lett.413 (2005) 454-457.

28. X. Chen, Y. Lou, A.C.S. Samia, C. Burda, J.L. Gole, Adv. Funct. Mater. 15 (2005) 41.
29. L. Lin, R.Y. Zheng, J.L. Xie, Y.X. Zhu, Y.C. Xie, Appl. Catal. B 76 (2007) 196.
30. M. Sathish, B. Viswanathan, R.P. Viswanath, C.S. Gopinath, Chem. Mater. 17 (2005)- 6349.
31. T. Ma, M. Akiyama, E. Abe, I. Imai, Nano Lett. 5 (2005) 2543.
32. R.Y. Zheng, Y. Guo, C. Jin, J.L. Xie, Y.X. Zhu, Y.C. Xie, J. Mol. Catal. A 2010, 319, 46.
33. R.Y. Zheng, L. Lin, J.L. Xie, Y.X. Zhu, Y.C. Xie, J. Phys. Chem. C 2008, 112, 15502.
34. Y.Y. Lv, L.S. Yu, H.Y. Huang, H.L. Liu, Y.Y. Feng, J. Alloys Compd. 2009, 488, 314.
35. S.C. Ke, T.C. Wang, M.S. Wong, N.O. Gopal, J. Phys. Chem. B 110 (2006) 11628-11634.
36. C.P. Kumar, N.O. Gopal, T.C. Wang, M.S. Wong, S.C. Ke, J. Phys. Chem. B 110 (2006) 5223-5229.
37. S. Livraghi, M.C. Paganini, E. Giamello, A. Selloni, C. Di Valentin, G. Pacchioni, Journal of the American Chemical Society 128 (2006) 15666-15671.
38. A.E. Giannakas, E. Seristatidou, Y. Deligiannakis, I. Konstantinou, Applied Catalysis B: Environmental 132- 133 (2013) 460- 468.
39. Y. Xie, X. Zhao, Y. Li, Q. Zhao, X. Zhou, Q. Yuan, Journal of Solid State Chemistry 181 (2008) 1936-1942.
40. Y. Nakaoka, Y. Nosaka J. Photochem. Photobiol. A: Chem. 110 (1997) 299.